ACS SyntheticBiology

pubs.acs.org/synthbio

Letter

Analysis of Three Architectures for Controlling PTP1B with Light

Akarawin Hongdusit,[#] Evan T. Liechty,[#] and Jerome M. Fox*

Cite This: *ACS Synth. Biol.* 2022, 11, 61−68

Read Online

ACCESS | Metrics & More | Article Recommendations | Supporting Information

ABSTRACT: Photosensory domains are powerful tools for placing proteins under optical control, but their integration into light-sensitive chimeras is often challenging. Many designs require structural iterations, and direct comparisons of alternative approaches are rare. This study uses protein tyrosine phosphatase 1B (PTP1B), an influential regulatory enzyme, to compare three architectures for controlling PTPs with light: a protein fusion, an insertion chimera, and a split construct. All three designs permitted optical control of PTP1B activity *in vitro* (i.e., kinetic assays of purified enzyme) and in mammalian cells; photoresponses measured under both conditions, while different in magnitude, were linearly correlated. The fusion- and insertion-based architectures exhibited the highest dynamic range and maintained native localization patterns in mammalian cells. A single insertion architecture enabled optical control of both PTP1B and TCPTP, but not SHP2, where the analogous chimera was active but not photoswitchable. Findings suggest that PTPs are highly tolerant of domain insertions and support the use of *in vitro* screens to evaluate different optogenetic designs.

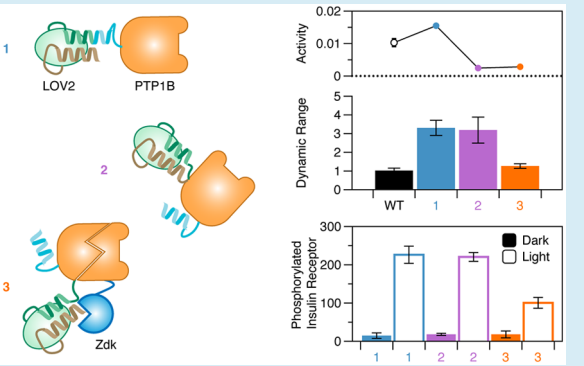

KEYWORDS: *optogenetics, protein engineering, signaling, protein tyrosine phosphatases, light-oxygen-voltage domains*

Optogenetics—the use of light-sensitive proteins to place biochemical events under optical control—has enabled detailed studies of cell signaling.[1−3] Light-activated protein kinases, in particular, have uncovered sophisticated mechanisms of signal integration and processing (e.g., low-pass filtering and fast feedback in the Ras/Erk mitogen-activated protein kinase cascade[1,4]) that would be difficult to resolve with bulk chemical perturbations (e.g., inhibitors[5]). Optical control of protein phosphatases, by contrast, has proven difficult to achieve;[6] light-sensitive analogues of these enzymes define an important gap in the modern optogenetic toolkit.

Protein phosphatases have conserved active sites that make them difficult to study with selective inhibitors (i.e., they are poor targets for chemical genetics[7,8]). Two recent studies have developed methods for controlling these enzymes with light. The first used photocaged amino acids to attenuate the activity and binding affinity of MAPK phosphatase 3 (MAP3 or DUSP6, which acts on phosphorylated tyrosine and threonine residues[6]). This strategy, which exploits common catalytic motifs, has the potential to be generalizable, but its reagent requirement (i.e., artificial amino acids), irreversibility, and use of ultraviolet light may hinder its application to studies of complex signaling dynamics (e.g., oscillations[9]) or layered tissues.[10] In a second study, our group placed protein tyrosine phosphatase 1B (PTP1B) under optical control by attaching its C-terminal α7 helix—an allosteric switch—to the N-terminal helix of the light-oxygen-voltage 2 (LOV2) domain from *Avena sativa* phototropin 1. For background, LOV2 binds a flavin mononucleotide (FMN) that forms a covalent adduct between its isoalloxazine C4a and a nearby cysteine under blue light; the resulting complex destabilizes the N- and C-terminal helices of LOV2, causing them to "unwind". In general, LOV domains are valuable for their reversibility[11,12] and tunable light-state lifetimes.[13] In the case of the PTP1B−LOV2 fusion, biophysical analyses suggest that light-induced unwinding of LOV2 inhibits catalytic activity by destabilizing the α7 helix of PTP1B (Figure 1A).[14] This genetically encodable architecture is reversible and preserves the native structure, activity, and subcellular localization of PTP1B; its use of a unique allosteric control element (i.e., the α7 helix), however, hinders its extension to other PTPs.

In a follow-up study, we used our optogenetic design to compare the allosteric control systems of PTP1B and TCPTP.[15] TCPTP is the closest homologue of PTP1B; their catalytic domains share 70% sequence identity, and they have overlapping regulatory targets, notably the insulin receptor (IR) and epidermal growth factor receptor (EGFR).[16] Our study began with an interesting observation: The fusion of LOV2 to the C-terminal helix of TCPTP does not permit

Received: August 19, 2021
Published: December 13, 2021

https://doi.org/10.1021/acssynbio.1c00398
ACS Synth. Biol. 2022, 11, 61−68

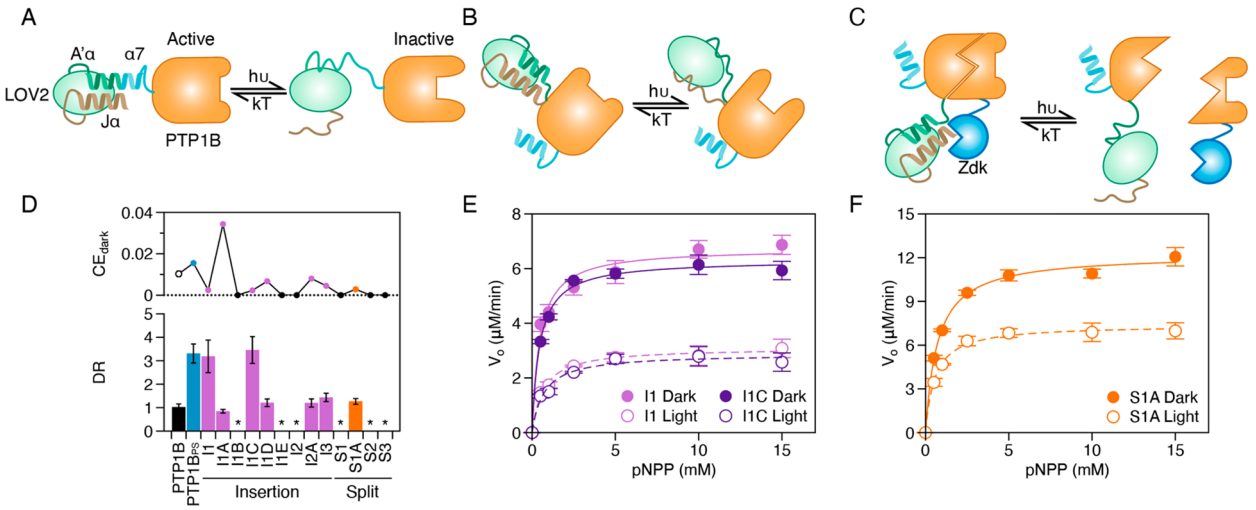

Figure 1. Development of alternative optogenetic architectures for PTP1B. (A) A depiction of $PTP1B_{PS}$. In this fusion, the A′α helix of LOV2 is connected to the allosterically influential α7 helix of PTP1B. Illumination of LOV2 with blue light causes its terminal helices to unwind, destabilizes the α7 helix of PTP1B, and disrupts catalytic activity.[14] (B) The design concept for an "insertion" chimera: LOV2 is inserted within a flexible loop on the surface of PTP1B; illumination of LOV2 causes structural distortions in PTP1B that disrupt its catalytic activity. (C) The design concept for a "split" construct: Two halves of PTP1B are held together by a noncovalent LOV2-Zdk1 complex; illumination of LOV2 causes the heterodimeric complex to dissociate—or to undergo a conformational change caused by the dissociation of LOV2-Zdk1—and disrupts catalytic activity. (D) The dark-state catalytic efficiency ($CE_{dark} = [k_{cat}/K_M]_{dark}$) and the dynamic range ($DR = [k_{cat}/K_M]_{dark}/[k_{cat}/K_M]_{light}$) of various constructs. Constructs with an asterisk were either not active or not expressible in *E. coli*. (E,F) Initial rates of PTP-catalyzed hydrolysis of *p*-nitrophenyl phosphate (pNPP) by high-DR variants of the (E) insertion and (F) split constructs in the presence and absence of light (455 nm). Error bars show standard error of the mean (n = 3 independently prepared reactions). Table S1 provides source data.

photocontrol. In follow-up experiments, we found that replacing regions of TCPTP with homologous regions from PTP1B enhanced photoswitching. This work showed that the allosteric functionality of the α7 helix is not completely conserved across the PTP family and highlighted residues that can transfer this functionality to TCPTP. Interestingly, the most photoswitchable fusion—hereafter, $TCPTP_{PS}$—included 25 residues from the α4–α7 helices and E loop of PTP1B; these modifications did not alter the substrate specificity of TCPTP, but the work required to identify them was laborious.

This study explores alternative approaches for placing protein tyrosine phosphatases (PTPs) under optical control. PTPs regulate a diverse set of physiological processes and contribute to many diseases (e.g., cancer, autoimmunity, metabolic disorders, and neurological diseases[17,18]); photoswitchable analogues could find broad use. Using PTP1B as a model system, our study focuses on two questions: (i) How do different optogenetic architectures affect enzyme activity, photoswitchability, and subcellular localization? (ii) Does the highly conserved PTP domain facilitate the rapid extension of some architectures to other members of the PTP family?

These questions are relevant to many signaling enzymes, but they are often overlooked in the development of light-sensitive constructs (e.g., alternative optogenetic architectures are rarely compared); their answers could help resolve important design rules for building photoswitchable variants of PTPs and, perhaps, other enzymes.

RESULTS AND DISCUSSION

We expanded on our first photoswitchable variant of PTP1B—the PTP1B–LOV2 fusion, hereafter $PTP1B_{PS}$—by developing two alternative optogenetic designs: (i) a single-chain "insertion chimera" and (ii) a photodissociable "split construct". For the first design, we inserted LOV2 into flexible loops on the surface of the catalytic domain of PTP1B (residues 1–321); we speculated that light-induced unwinding of LOV2 would trigger activity-modulating structural distortions in the catalytic domain (Figure 1B). For the second construct, we divided the catalytic domain into two segments and attached each half to LOV2 or Zdk1. The LOV2-Zdk1 complex, termed "LOVTRAP", dissociates under blue light;[19] we speculated that it would permit optical control of PTP1B dissociation (Figure 1C). Prior work indicates that both architectures—an inserted light switch[20,21] and a photodimerizer[22−25]—are compatible with many proteins. Notably, we designed both constructs for optical inhibition, rather than activation, to address the absence of selective PTP inhibitors, which could be useful in chemical genetics.

We explored each of our optogenetic architectures by testing them at three sites. For the insertion construct, we chose (i) a minimally disruptive site, (ii) a maximally disruptive site, and (iii) a site likely to permit domain dissection (here, we define "disruption" as a structural perturbation that affects enzyme activity; Figure S1). We selected the first two sites by consulting a study of loop-insertion mutants. Here, researchers inserted a 25-residue segment into poorly conserved loops on PTP1B and measured its effect on catalytic activity;[26] we selected nondisruptive and disruptive sites. We chose the third site by using the Split Protein rEassembly by Ligand or Light (SPELL) portal, an online tool that uses a physical scoring function to predict functional split sites in proteins.[27] For all sites, we encouraged conformational coupling between the PTP1B and LOV2 domains by attaching them without a linker. For the split construct, we replaced the disruptive site—which could impede PTP1B assembly—with a second site from the SPELL portal (Figure S1). To avoid structural disruptions in the split constructs, we added a five-residue linker between each half of PTP1B and its fusion partner (i.e., LOV2 and Zdk).

https://doi.org/10.1021/acssynbio.1c00398
ACS Synth. Biol. 2022, 11, 61−68

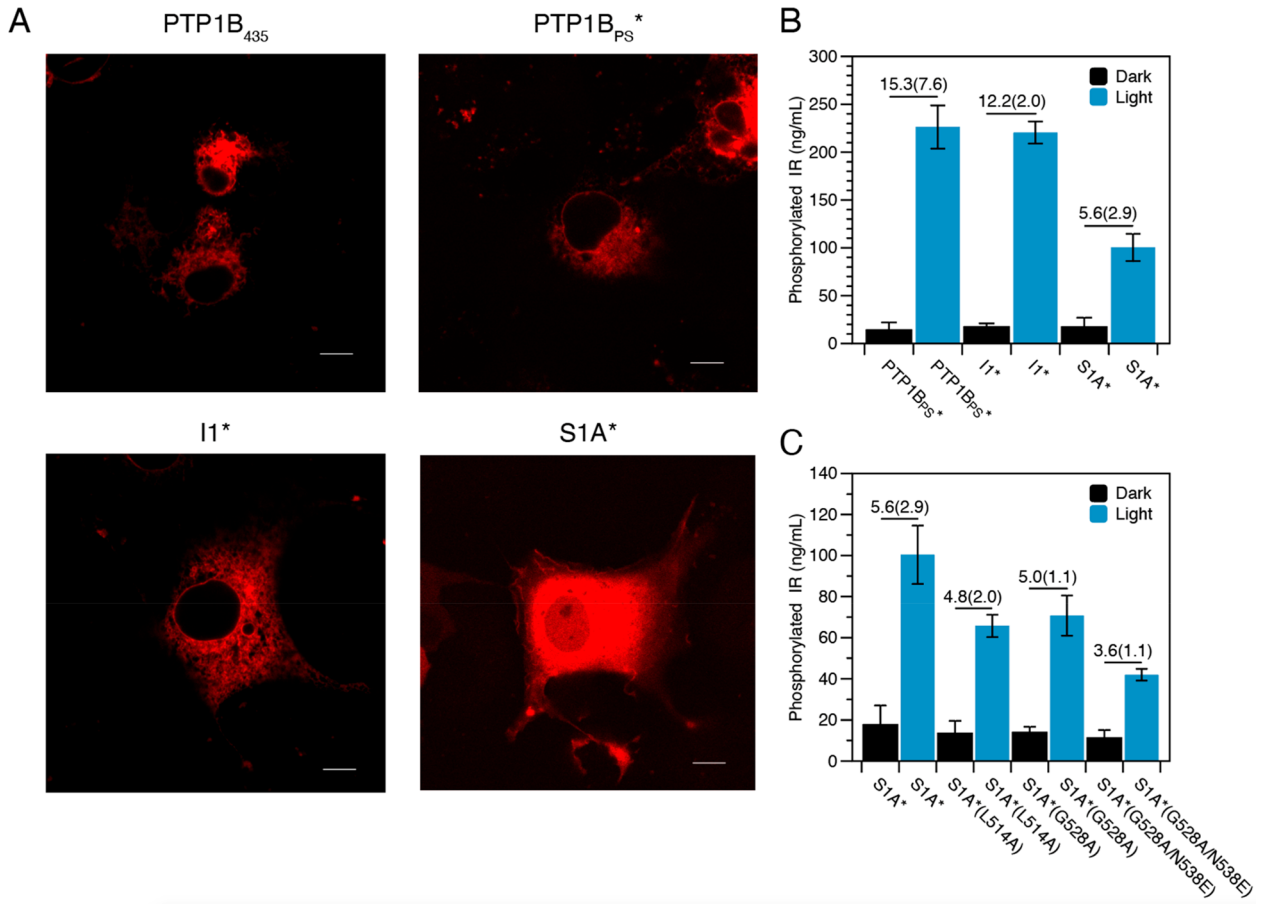

Figure 2. Analysis of natively localized constructs. (A) Images of COS-7 cells expressing RFP-tagged variants of PTP1B: $PTP1B_{435}$ is the wild-type protein, which contains a C-terminal region (a disordered proline-rich domain followed by a short membrane anchor) that localizes it to the endoplasmic reticulum (ER). $PTP1B_{PS}$* is a version of $PTP1B_{PS}$ that includes residues 299−435 from the wild-type enzyme attached to its C-terminus; I1* and S1A* include the same region of the full-length enzyme. $PTP1B_{435}$, $PTP1B_{PS}$*, and I1* exhibit indistinguishable localization patterns that are consistent with localization to the ER; for S1A*, fluorescence in the cytosol suggests that a significant fraction of its N-terminal half (i.e., RFP-PTP1B-Zdk1) is dissociated from its C-terminal half (i.e., ER-localized LOV2-PTP1B; scale bar, 10 μm). Additional images appear in Figure S3. (B,C) ELISA-based measurements of IR phosphorylation in HEK293T/17 stably expressing variants of PTP1B after 10 min exposure to light (455 nm) or darkness. The DR (i.e., the ratio of light- to dark-state signals) appears above the bars for each construct. (B) Illumination increases IR phosphorylation for all constructs. (C) The introduction of LOV2-stabilizing mutations does not improve the dynamic range of S1A*. The plotted data depict the mean and SE for measurements of n = 3 biological replicates. The error in DR depicts propagated SE for n = 3 biological replicates under each condition (light and dark). Source data appear in Table S6.

We characterized all constructs by using *in vitro* kinetic assays. In brief, we assayed the activity of purified proteins on *p*-nitrophenyl phosphate (pNPP) in the presence and absence of light, and we used initial rates to construct dark- and light-state Michaelis−Menten curves (Figure S2, Table S1). All three insertion chimeras expressed in *E. coli*, and one—hereafter, I1—showed light-sensitive catalytic activity; all split constructs failed to express (Figure 1D,E). Noting that fusion partners often alter the expression levels of their companion proteins,[28,29] we swapped the LOV2 and Zdk domains in S1, a split construct with the same insertion site as I1. The resulting construct, termed S1A, expressed well in *E. coli* and showed light-sensitive catalytic activity (Figure 1D,F). Our initial analysis of different chimeras indicates that both insertion and split architectures permit photocontrol of PTPs.

We estimated the dynamic range (DR) of different constructs by using eq 1, where k_{cat}/K_M is an apparent second order rate constant; this parameter, which is often referred to as

$$\mathrm{DR} = \frac{[k_{cat}/K_M]_{dark}}{[k_{cat}/K_M]_{light}} \quad (1)$$

catalytic efficiency (CE), is particularly relevant at low substrate concentrations (i.e., $[S] \ll K_M$), a reasonable intracellular condition.[30,31] The DRs of $PTP1B_{PS}$ and I1 were indistinguishable from one another and much larger than that of S1A (Figure 1D). $PTP1B_{PS}$ uses a native allosteric switch (the α7 helix) that can modulate catalytic activity by up to ∼3-fold.[14] I1, by contrast, relies on a non-native conformational change; we speculated that its architecture might permit enhanced photoswitching. To improve the DR of I1, we modified LOV2 by adding (i) one- and five-residue linkers to both sides, (ii) a five-residue linker to one side, or (iii) mutations that stabilize its dark state (Table 1); similar structural modifications have improved the DRs of other light-sensitive proteins.[32] For the one-residue linker, we used a single glycine residue, which we chose for its flexibility and generally nondisruptive influence on loop structure.[33] For the five-residue linker, we used the first five residues of the 25-

https://doi.org/10.1021/acssynbio.1c00398
ACS Synth. Biol. 2022, 11, 61−68

residue segment used in the aforementioned study of "loop-insertion" mutants.[26] We reasoned that these five-residues would not disrupt enzyme function. Intriguingly, none of our modifications improved the DR of PTP1B; all but one—a five-residue linker downstream of LOV2 (I1C)—reduced photoswitching, dramatically reduced expression, or inactivated the enzyme. Our modification of I1 illustrates the challenge of using rational changes to improve the DR of light-sensitive enzymes, particularly those that rely on allosteric control.

Proteins inserted on the surface of PTP1B (i.e., LOV2 or the LOV2-Zdk complex) are, perhaps, more likely to alter its activity than simple fusions (e.g., $PTP1B_{PS}$). We compared the activity of each construct by using the dark-state CE (Figure 1D). We observed no correlation between enzyme activity and DR. Intriguingly, most new constructs (i.e., I and S) had a lower activity than the wild-type enzyme, but one—I1A, which has five-residue linkers on both sides of LOV2—had a 3-fold higher CE. Our kinetic data thus indicate that domain insertions have a greater influence on PTP1B activity than simple fusions but suggest that they can enhance or inhibit catalysis, depending on small differences in insertion architecture (e.g., linker length).

The full-length version of PTP1B possesses a C-terminal disordered region (residues 322−405) followed by a short anchor (residues 406−435) that localizes it to the endoplasmic reticulum (ER) of mammalian cells. We prepared I1 and S1A for imaging in COS-7 cells by adding both (i) the native C-terminal region of PTP1B (residues 322-435) and (ii) an N-terminal fluorescent tag (i.e., red fluorescent protein, or RFP). The full-length versions of our photoswitchable constructs are denoted $PTP1B_{PS}$*, I1*, and S1A*. Like $PTP1B_{PS}$*, chimera I1* exhibited a native localization pattern; for S1A*, by contrast, we observed fluorescence in the cytosol, an indication that some of its fluorescently labeled N-terminal half (i.e., RFP-PTP1B-Zdk1) is not complexed with its C-terminal half (i.e., ER-localized LOV2-PTP1B; Figure 2A and Figure S3). This incomplete dark-state assembly of S1A* may result from the interference of PTP1B with the interaction between the C-terminal Jα helix of LOV2 and the Zdk1 domain,[19] and probably contributes to its low DR. We note: The photoresponse of S1A in kinetic assays does not necessarily indicate that this construct dissociates under blue light; after all, LOV2 is inserted at a site where conformational changes alone can disrupt catalytic activity (e.g., I1). By showing that a sizable fraction of S1A is already dissociated in the dark state, however, our imaging experiments suggest that this construct is likely to dissociate further under blue light (which further reduces LOV2-Zdk1 binding affinity).

We evaluated the control afforded by I1* and S1A* by using them to dephosphorylate the insulin receptor (IR), a membrane-bound regulatory target of PTP1B. In brief, we generated HEK293T/17 cells that stably express $PTP1B_{PS}$*, I1*, and S1A*, and we used an enzyme-linked immunosorbent assay (ELISA) to measure shifts in IR phosphorylation caused by transient illumination (455 nm, 10 min). $PTP1B_{PS}$*, which we characterized in detail in prior work, served as a positive control. To our satisfaction, both I1* and S1A* enhanced IR phosphorylation in the light and left phosphorylation levels unaltered in the dark (Figure 2B and Figure S4A,B). By contrast, light-insensitive mutants of all three constructs exhibited no photoresponse and yielded phosphorylation levels that were indistinguishable from wild-type PTP1B (Figure S4A,B). This finding suggests that an active form of LOV2 is required for a measurable photoresponse. Like $PTP1B_{PS}$*, I1* produced large shifts (∼12-fold) in IR phosphorylation. S1A* was less influential (∼6-fold)—perhaps a result of its lower DR; mutations that stabilize the dark state of LOV2 did not improve the DR further (Figure 2C). The large shifts afforded by these constructs are surprising and evidence a hypersensitivity to PTP1B activity that merits further exploration. Importantly, prior work on light-sensitive kinases suggests that the DRs afforded by our constructs in cells (6- to 15-fold) are sufficient to enable quantitative analyses of downstream signaling events.[4] Altogether, $PTP1B_{PS}$*, I1*, and S1A* provide three alternative architectures for placing PTP1B-mediated signaling events under optical control.

The catalytic domains of PTPs have a highly conserved three-dimensional fold—a single domain of β sheets flanked by α helices.[34] To determine if the I1 architecture, which required no optimization, could be readily extended to other PTPs, we inserted LOV2 into homologous sites on TCPTP and SHP2 (Figure 3A). The catalytic domains of these enzymes share 70% and 30% amino acid sequence identity, respectively, with the catalytic domain of PTP1B.[35] Unfortunately, the TCPTP−LOV2 chimera ($TCPTP_{I1}$) failed to express in *E. coli* at yields compatible with facile purification (i.e., cell lysis followed by standard nickel-affinity purification did not yield detectable protein), and the SHP2 analogue ($SHP2_{I1}$) did not exhibit light-dependent catalytic activity, though the enzyme remained active (Figure 3B). We did not pursue SHP2 in cell-based studies.

We focused further development on TCPTP. Like PTP1B, this enzyme is a negative regulator of IR phosphorylation. It has two main isoforms: an ER-bound 48-kDa variant (TC48) and a nuclear 45-kDa variant (TC45).[36] We attached the ER-targeting region (residues 318−415) of TC48 to the C-terminus of three chimeras: $TCPTP_{PS}$, $TCPTP_{I1}$, and $TCPTP_{I2}$. $TCPTP_{PS}$ was not characterized in mammalian cells; $TCPTP_{I1}$ and $TCPTP_{I2}$ include minimally and maximally disruptive architectures and thus provide contrasting structural alternatives. As above, we denote our ER-targeting chimeras as $TCPTP_{PS}$*, $TCPTP_{I1}$* and $TCPTP_{I2}$*. Both $TCPTP_{PS}$* and $TCPTP_{I1}$* increased IR phosphorylation in HEK293T/17 cells by 8- and 9-fold, respectively; $TCPTP_{I2}$* showed no photoresponse (Figure 3C). The activity of $TCPTP_{I1}$* is surprising, given the poor expression of $TCPTP_{I1}$ in *E. coli*. Previous studies of mammalian protein expression in *E. coli* have struggled to yield general rules for high-yield expression;[37] this particular construct, which lacks essential post-translational modifications or disulfide bonds, may benefit from eukaryotic chaperones. As with our PTP1B−LOV2 chimeras, phosphorylation levels in the dark were indistinguishable between all constructs (Figure S4A).

We completed our analysis of PTP chimeras by comparing photoresponses from *in vitro* kinetic studies and cell-based assays. Intriguingly, estimates of DR from both sets of experiments were linearly correlated (R^2 = 0.94; Figure S4D); differences in photoswitching observed *in vitro* appear to be conserved in mammalian cells. This conservation is consistent with findings from a prior study of light-inducible dimers, for which dark- and light-state binding affinities measured *in vitro* correlated with activity changes in cell-based assays (e.g., transcription and localization).[38]

This study develops two new optogenetic architectures for PTP1B—an insertion chimera and a split construct—and compares them with a third, previously developed fusion. The

https://doi.org/10.1021/acssynbio.1c00398
ACS Synth. Biol. 2022, 11, 61−68

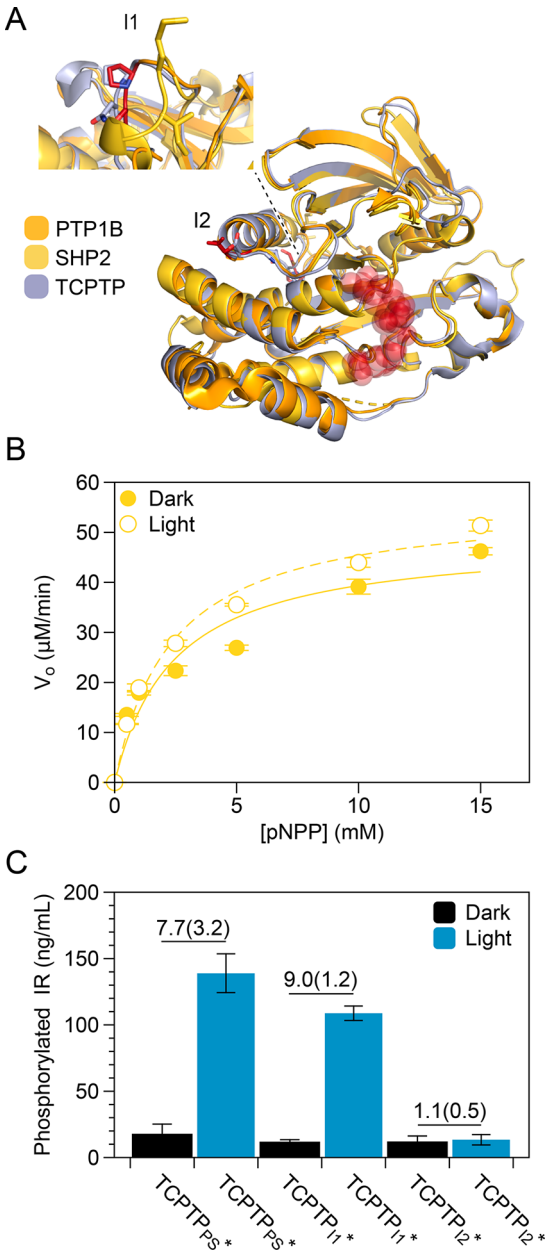

Figure 3. Extension of the insertion-based approach to other PTPs. (A) Aligned crystal structures of the catalytic domains of PTP1B, SHP2, and TCPTP (pdb entries 2cm2, 3zm1, and 1l8k, respectively). Highlights: competitive inhibitor (red spheres, pdb entry 2f71), insertion site I1 ($PTP1B_{205-206}$, $TCPTP_{206-207}$, and $SHP2_{449-450}$; red sticks), and insertion site I2 ($PTP1B_{186-187}$, red sticks). (B) Initial rates of $SHP2_{I1}$-catalyzed hydrolysis of pNPP in the presence and absence of light (455 nm). Values of k_{cat} and K_M are indistinguishable ($p < 0.05$). (C) ELISA-based measurements of IR phosphorylation in HEK293T/17 cells stably expressing photoswitchable variants of TCPTP after 10 min exposure to light (455 nm) or darkness. $TCPTP_{PS}$* is a version of $TCPTP_{PS}$ that includes residues 318−415 from the wild-type enzyme (i.e., the ER anchor) attached to its C-terminus; $TCPTP_{I1}$* and $TCPTP_{I2}$* include the same region of the full-length enzyme. Illumination increases IR phosphorylation for $TCPTP_{PS}$* and $TCPTP_{I1}$*, but not $TCPTP_{I2}$*. The plotted data depict the mean and SE for measurements of $n = 3$ biological replicates. The DR appears above the bars for each construct; here, error depicts propagated SE for $n = 3$ biological replicates under each condition (light and dark). Tables S1 and S6 provide source data.

two new designs disrupted enzyme activity more than the fusion but, nonetheless, enabled optical control of PTP1B activity in human cells. The insertion chimera exhibited the highest DR (which was indistinguishable from the DR of the fusion) and maintained native subcellular localization in COS-7 cells. This architecture was also compatible with TCPTP, but not SHP2, suggesting that the sensitivity of PTPs to specific insertion points cannot be generalized across the PTP family. The photoswitchable variants of TCPTP examined in this study—the first characterized in mammalian cells—could support future studies of functional redundancy between TCPTP and PTP1B, an incompletely understood phenomenon.[16,39] The active SHP2−LOV2 chimera, in turn, provides a promising starting point for building photoswitchable analogues; shorter loops between SHP2 and LOV2, for example, might enhance photoswitching in future constructs.

Our findings provide important guidance for the development of photoswitchable PTPs and, perhaps, other photoswitchable enzymes, though the generality of our results must be tested. First, they suggest that photoresponses measured in kinetic studies of purified enzymes and cell-based assays can be highly correlative (Figure S4D); this finding supports the use of *in vitro* assays to test and optimize optogenetic designs. Second, they show that the influence of rational changes in optogenetic architectures is difficult to predict; mutations in LOV2 that enhance the DR of some constructs, for example, may fail to do so in others. Third, they indicate that PTPs, which include broad allosteric networks,[40] may be particularly compatible with domain insertions; the extension of specific insertion-based architectures to other family members, however, may still require the assembly of several structural variants. Finally, and most intriguingly, they suggest that alternative allosteric control systems involving the same combination of proteins (e.g., PTP1B and LOV2) may exhibit maximal DRs (e.g., consider the DRs of $PTP1B_{PS}$, I1, I1C). This limiting behavior motivates the examination of alternative optogenetic actuators in future efforts to develop photoswitchable enzymes.

METHODS

Materials. We purchased Turbo and BL21(DE3) *E. coli* cells from New England Biolabs (Ipswich, MA); *p*-nitrophenyl phosphate (pNPP) and activated insulin receptor from MilliporeSigma (St. Louis, MO); gBlocks (gene fragments) from Integrated DNA Technologies (Coralville, IA); a 455 nm light from Mightex Systems (Pleasanton, CA); BBR [(3-(3,5-dibromo-4-hydroxybenzoyl)-2-ethyl-*N*-[4-[(2-thiazolylamino)-sulfonyl]phenyl]-6-benzofuransulfonamide] from Cayman Chemical (Ann Arbor, MI); PathScan Phospho-Insulin Receptor β (panTyr) Sandwich ELISA Kit from Cell Signaling Technology (Danvers, MA); and all other reagents from MilliporeSigma or Thermo Fisher.

Cloning and Molecular Biology. We ordered the genes encoding engineered phosphatases from Integrated DNA Technologies, and we used Gibson Assembly to insert the genes into a pET16b vector. Briefly, we PCR-amplified the gene with 45−50 °C overhangs at both 5′ and 3′ ends complementary to the MCS of the vector. We incubated the DNA fragments in Gibson Assembly master mix at 50 °C for 1 h and used 5 μL of the mixture to transform Turbo competent *E. coli* cells (NEB) with heat shock. We spread the cells onto an agar plate (25 g/L LB, 100 mg/L carbenicillin, 1.5% agar) and incubated the plate overnight at 37 °C. We inoculated the

https://doi.org/10.1021/acssynbio.1c00398
ACS Synth. Biol. 2022, 11, 61−68

liquid culture overnight and extracted the plasmid DNA using a DNA extraction kit (Omega Biotek). The Supporting Information includes amino acid sequences of all constructs (Table S2), primers for Gibson assembly (Table S3), gBlock sequences (Table S4), and primers used for site-directed mutagenesis (Table S5).

Protein Expression and Purification. We overexpressed polyhistidine-tagged versions of various constructs (Table S2) by performing the following steps: (i) We used heat shock to transform BL21 (DE3) *E. coli* cells (NEB) with each pET16b vector, spread the cells onto an agar plate (25 g/L LB, 100 mg/L carbenicillin, 1.5% agar), and incubated the plate at 37 °C for 12 h. (ii) We inoculated a 20 mL LB culture (25 g/L LB, 100 mg/L carbenicillin) with a single colony and incubated the culture for 5 h. (iii) We inoculated 1 L of induction media (20 g/L tryptone, 10 g/L yeast extract, 5 g/L NaCl, 4 g/L M9 salts, 4 g/L glucose, and 100 mg/L carbenicillin) with the 20 mL culture and incubated at 37 °C until the OD_{600} reached 0.5−0.8. (iv) We added 500 μL of 1 M solution of isopropyl β-D-1-thiogalactopyranoside (IPTG) to the 1 L culture, reduced the temperature to 22 °C, and incubated the culture for 18−20 h. (v) We spun down the cells after 18−20 h of incubation at 3950*g* for 20 min using a JA-10 Beckman Coulter centrifuge.

We purified all proteins with ÄKTA pure fast protein liquid chromatography (FPLC, GE Healthcare) by carrying out the following steps. (i) We lysed the cells with the following solution (per gram of cell pellet): 4 mL of B-PER (Thermo Fisher Scientific, Inc.), 1 mg of $MgSO_4$, 2 mg of Nα-*p*-tosyl-L-arginine methyl ester hydrochloride, 1.25 mg of tris(2-carboxyethyl)phosphine (TCEP), 3.75 μL of phenylmethylsulfonyl fluoride, 1 mg of lysozyme, and 10 μL of DNase. We mixed the lysis mixture to homogeneity and rocked it at room temperature (∼22 °C) for 1 h. (ii) We pelleted the cells at 3950*g* for 25 min and removed the cell debris. (iii) We clarified the supernatant by adding a saturated solution of ammonium sulfate to 10% (v/v), pelleted the precipitate at 3950*g* for 15 min and filtered the supernatant with 0.22-μm filter. (iv) We ran our supernatant over an Ni column (HisTrap HP, GE Healthcare) and eluted the protein using 0−100% gradient of imidazole (50 mM Tris-HCl, 0.5 mM TCEP, 500 mM imidazole, pH 7.5). (v) We purified the protein further on an anion exchange column (HiPrep Q HP 16/10, GE Healthcare). Here, we eluted the final protein using a 0−100% gradient of NaCl for 1 h (50 mM HEPES, 0.5 mM TCEP, 500 mM NaCl, pH 7.5). (vi) We performed SDS-PAGE on the eluant fractions to assess purity and stored the protein in storage buffer (50 mM HEPES, 0.5 mM TCEP, 20% v/v glycerol, pH 7.5) at −80 °C.

Analysis of Photoswitching. For each purified construct, we measured PTP-catalyzed hydrolysis of pNPP in the presence and absence of light. Each reaction consisted of the following mixture: enzyme (100 nM), pNPP (0.5, 1, 2.5, 5, 10, 15 mM), and buffer (50 mM HEPES and 0.5 mM TCEP, pH 7.3). We performed the assay at room temperature (22 °C) in the presence and absence of 455 nm light and measured the absorbance at 405 nm at 4, 8, and 12 min after reaction initiation on a Spectramax M2 plate reader. Table S1 includes all kinetic constants.

Preparation of Cells for Imaging Experiments. We grew COS-7 cells (ATCC CRL-1651) in DMEM media (10% FBS, 100 units/mL penicillin G sodium, and 100 μg/mL streptomycin sulfate) for ∼24 h to achieve 70−90% confluency, and we seeded them on a 20 mm MatTek dish. At ∼24 h after seeding, we transfected the cells with 2500 ng of plasmid DNA and 7.5 μL of Lipofectamine 3000 reagent (Invitrogen) according to the manufacturer's protocols. At 14−16 h after transfection with plasmid DNA, we imaged the cells at 37 °C.

Confocal Microscopy. We carried out all imaging experiments with a 100× 1.45 NA oil objective on a Nikon A1R confocal scanning microscope equipped with an environmental chamber (37 °C, 75% humidity, and 5% CO_2; Pathology Devices, Inc.). To localize RFP-tagged chimeras, we illuminated COS-7 cells with a 561 nm laser (pixel dwell time of 2.2 μs) and imaged them with a 605/50 nm bandpass filter.

Preparation of Cells for Enzyme-Linked Immunosorbent Assay (ELISA). For our *in vitro* cell studies, we generated HEK293T/17 cells that express the following constructs: $PTP1B_{PS}$*, I1*, S1A*, S1A*(L514A), S1A*(G528A), S1A*(G528A/N538E), $TCPTP_{PS}$*, $TCPTP_{I1}$*, and $TCPTP_{I2}$*. Briefly, we grew HEK293T/17 cells in 75 cm^2 flasks (Corning) in DMEM media with 10% FBS, 100 units/mL penicillin G sodium and 100 μg/mL streptomycin sulfate. We transfected the cells using Lipofectamine 3000 (Invitrogen) and plasmid DNA (i.e., pAcGFP1-C1 containing the gene of interest, no gene for GFP, and neomycin resistant gene replaced with puromycin resistant gene) according to the manufacturer's protocols. We passaged the cells with DMEM media (as above) supplemented with 1.5 μg/mL puromycin and replaced media when the cells reached 60−90% confluency. We froze the cells after seven passages.

Enzyme-Linked Immunosorbent Assay (ELISAs). We performed ELISA to measure the phosphorylation of IR under different conditions. To begin, we depleted endogenous PTP1B or TCPTP with 25 nM siRNA (AM16794 and s11509, respectively; Thermo Fisher Scientific) and 12.5 μL of Dharmafect (Dharmacon), according to manufacturer protocols. We starved the cells for 48 h with FBS-free media. We exposed cells to (i) 455 nm light, (ii) total darkness, or (iii) 300 μM of BBR for 10 min and immediately removed the media and lysed the cell in lysis buffer (Cell Signaling Technology) supplemented with 1X halt phosphatase inhibitor and 1X halt protease inhibitor (Thermo Fisher Scientific) for 10 min. We spun the cells down, collected the supernatant, and diluted the samples to 30 mg/mL for the PathScan Phospho-Insulin Receptor β (panTyr) Sandwich ELISA Kit (Cell Signaling Technology; #7082).

We carried out ELISA according to the manufacturer's protocols. In brief, we prepared the antibody solutions by dissolving the lyophilized primary antibody (phospho-tyrosine mouse detection mAb; #12982) and secondary antibody (antimouse IgG, HRP-linked antibody; #13304) in their respective buffers (#13339 and #13515). Next, we prepared 100 μL of 1-, 2-, 4-, and 8-fold dilutions of each sample and incubated each sample in a single well of antibody-coated 96-well plate overnight at 4 °C. We washed the wells four times with 1X wash buffer and incubated the wells with 100 μL of primary antibody solution at 37 °C for 1 h, repeated the wash steps, and incubated with 100 μL of secondary antibody solution at 37 °C for 30 min. We washed the wells and incubated them with 100 μL of TMB substrate at 37 °C for 10 min, added a STOP solution, and measured the absorbance at 450 nm using the SpectraMax M2 plate reader. Finally, we converted raw absorbance values to estimates of the concentration of phosphorylated insulin receptor by using a

https://doi.org/10.1021/acssynbio.1c00398
ACS Synth. Biol. 2022, 11, 61−68

standard curve, prepared with a purified sample of phosphorylated insulin receptor (MilliporeSigma; #14-803) in lysis buffer (Cell Signaling Technology; #9803). Table S6 includes all ELISA data.

Statistical Analysis and Reproducibility. We determined statistical significance (Figure S4) with a two-tailed Student's *t* test.

■ ASSOCIATED CONTENT

Supporting Information

The Supporting Information is available free of charge at https://pubs.acs.org/doi/10.1021/acssynbio.1c00398.

Supplementary figures detailing insertion sites for photoswitchable chimeras and the workflow for the photoswitching assay; data for imaging experiments, enzyme-linked immunosorbent assay (ELISAs), and *in vitro* kinetic studies; amino acid sequences for PTP-LOV2 constructs; primers and gBlock sequences used for DNA assembly; supplementary references (PDF)

Table S6 provides ELISA-based measurements of insulin receptor phosphorylation (XLSX)

■ AUTHOR INFORMATION

Corresponding Author

Jerome M. Fox − *Department of Chemical and Biological Engineering, University of Colorado Boulder, Boulder, Colorado 80303, United States;* orcid.org/0000-0002-3739-1899; Email: jerome.fox@colorado.edu

Authors

Akarawin Hongdusit − *Department of Chemical and Biological Engineering, University of Colorado Boulder, Boulder, Colorado 80303, United States*

Evan T. Liechty − *Department of Chemical and Biological Engineering, University of Colorado Boulder, Boulder, Colorado 80303, United States*

Complete contact information is available at: https://pubs.acs.org/10.1021/acssynbio.1c00398

Author Contributions

#A.H. and E.T.L. contributed equally to this work. A.H., E.T.L., and J.M.F. conceived of the research. A.H., E.T.L., and J.M.F. designed experiments. A.H. assembled, purified, and assayed protein chimeras. A.H. and E.T.L. carried out imaging experiments and ELISAs. All authors analyzed data. All authors wrote the paper.

Notes

The authors declare no competing financial interest.

■ ACKNOWLEDGMENTS

This work was supported by funds provided by the National Science Foundation (A.H. and J.M.F., award 1804897) and the National Institute Of General Medical Sciences of the National Institutes of Health (E.T.L., award R35GM143089). The content is solely the responsibility of the authors and does not necessarily represent the official views of the National Institutes of Health.

■ REFERENCES

(1) Toettcher, J. E.; Weiner, O. D.; Lim, W. A. Using optogenetics to interrogate the dynamic control of signal transmission by the Ras/Erk module. *Cell* **2013**, *155*, 1422−1434.

(2) Van Haren, J.; Charafeddine, R. A.; Ettinger, A.; Wang, H.; Hahn, K. M.; Wittmann, T. Local control of intracellular microtubule dynamics by EB1 photodissociation. *Nat. Cell Biol.* **2018**, *20*, 252−261.

(3) Kim, N.; Kim, J. M.; Lee, M.; Kim, C. Y.; Chang, K. Y.; Heo, W. Do. Spatiotemporal control of fibroblast growth factor receptor signals by blue light. *Chem. Biol.* **2014**, *21*, 903−912.

(4) Zhou, X. X.; Fan, L. Z.; Li, P.; Shen, K.; Lin, M. Z. Optical control of cell signaling by single-chain photoswitchable kinases. *Science (Washington, DC, U. S.)* **2017**, *355*, 836−842.

(5) Bantscheff, M.; Eberhard, D.; Abraham, Y.; Bastuck, S.; Boesche, M.; Hobson, S.; Mathieson, T.; Perrin, J.; Raida, M.; Rau, C.; Reader, V.; Sweetman, G.; Bauer, A.; Bouwmeester, T.; Hopf, C.; Kruse, U.; Neubauer, G.; Ramsden, N.; Rick, J.; Kuster, B.; Drewes, G. Quantitative chemical proteomics reveals mechanisms of action of clinical ABL kinase inhibitors. *Nat. Biotechnol.* **2007**, *25*, 1035−1044.

(6) Courtney, T. M.; Deiters, A. Optical control of protein phosphatase function. *Nat. Commun.* **2019**, *10*, 1−10.

(7) Stanford, S. M.; Bottini, N. Targeting Tyrosine Phosphatases: Time to End the Stigma. *Trends Pharmacol. Sci.* **2017**, *38*, 524.

(8) Zhang, S.; Zhang, Z. Y. PTP1B as a drug target: recent developments in PTP1B inhibitor discovery. *Drug Discovery Today* **2007**, *12*, 373−381.

(9) Violin, J. D.; Zhang, J.; Tsien, R. Y.; Newton, A. C. A genetically encoded fluorescent reporter reveals oscillatory phosphorylation by protein kinase C. *J. Cell Biol.* **2003**, *161*, 899−909.

(10) Ruggiero, E.; Alonso-de Castro, S.; Habtemariam, A.; Salassa, L. Upconverting nanoparticles for the near infrared photoactivation of transition metal complexes: new opportunities and challenges in medicinal inorganic photochemistry. *Dalt. Trans.* **2016**, *45*, 13012−13020.

(11) Kennis, J. T. M.; van Stokkum, I. H. M.; Crosson, S.; Gauden, M.; Moffat, K.; van Grondelle, R. The LOV2 Domain of Phototropin:A Reversible Photochromic Switch. *J. Am. Chem. Soc.* **2004**, *126*, 4512−4513.

(12) He, L.; Tan, P.; Zhu, L.; Huang, K.; Nguyen, N. T.; Wang, R.; Guo, L.; Li, L.; Yang, Y.; Huang, Z.; Huang, Y.; Han, G.; Wang, J.; Zhou, Y. Circularly permuted LOV2 as a modular photoswitch for optogenetic engineering. *Nat. Chem. Biol.* **2021**, *17*, 915−923.

(13) Zoltowski, B. D.; Vaccaro, B.; Crane, B. R. Mechanism-based tuning of a LOV domain photoreceptor. *Nat. Chem. Biol.* **2009**, *5*, 827.

(14) Hongdusit, A.; Zwart, P. H.; Sankaran, B.; Fox, J. M. Minimally Disruptive Optical Control of Protein Tyrosine Phosphatase 1B. *Nat. Commun.* **2020**, *11*, 788.

(15) Hongdusit, A.; Fox, J. Optogenetic Analysis of Allosteric Control in Protein Tyrosine Phosphatases. *Biochemistry* **2021**, *60*, 254−258.

(16) Tiganis, T. PTP1B and TCPTP - Nonredundant phosphatases in insulin signaling and glucose homeostasis. *FEBS J.* **2013**, *280*, 445.

(17) He, R.; Yu, Z.; Zhang, R.; Zhang, Z. Protein tyrosine phosphatases as potential therapeutic targets. *Acta Pharmacol. Sin.* **2014**, *35*, 1227−1246.

(18) Schickel, J. N.; Kuhny, M.; Baldo, A.; Bannock, J. M.; Massad, C.; Wang, H.; Katz, N.; Oe, T.; Menard, L.; Soulas-Sprauel, P.; Strowig, T.; Flavell, R.; Meffre, E. PTPN22 inhibition resets defective human central B cell tolerance. *Sci. Immunol.* **2016**, *1*, aaf7153.

(19) Wang, H.; Vilela, M.; Winkler, A.; Tarnawski, M.; Schlichting, I.; Yumerefendi, H.; Kuhlman, B.; Liu, R.; Danuser, G.; Hahn, K. M. LOVTRAP: An optogenetic system for photoinduced protein dissociation. *Nat. Methods* **2016**, *13*, 755−758.

(20) Dagliyan, O.; Tarnawski, M.; Chu, P.-H.; Shirvanyants, D.; Schlichting, I.; Dokholyan, N. V.; Hahn, K. M. Engineering extrinsic disorder to control protein activity in living cells. *Science (Washington, DC, U. S.)* **2016**, *354*, 1441−1444.

(21) Shaaya, M.; Fauser, J.; Zhurikhina, A.; Conage-Pough, J. E.; Huyot, V.; Brennan, M.; Flower, C. T.; Matsche, J.; Khan, S.; Natarajan, V.; Rehman, J.; Kota, P.; White, F. M.; Tsygankov, D.; Karginov, A. V.; Larrondo, L. F.; Cooper, J. A.; Larrondo, L. F. Light-

regulated allosteric switch enables temporal and subcellular control of enzyme activity. *Elife* **2020**, *9*, No. e60647.
(22) Kennedy, M. J.; Hughes, R. M.; Peteya, L. A.; Schwartz, J. W.; Ehlers, M. D.; Tucker, C. L. Rapid blue-light-mediated induction of protein interactions in living cells. *Nat. Methods* **2010**, *7*, 973−975.
(23) Taslimi, A.; Zoltowski, B.; Miranda, J. G.; Pathak, G. P.; Hughes, R. M.; Tucker, C. L. Optimized second-generation CRY2-CIB dimerizers and photoactivatable Cre recombinase. *Nat. Chem. Biol.* **2016**, *12*, 425−430.
(24) Tarutina, M.; Ryjenkov, D. A.; Gomelsky, M. An unorthodox bacteriophytochrome from Rhodobacter sphaeroides involved in turnover of the second messenger c-di-GMP. *J. Biol. Chem.* **2006**, *281*, 34751−34758.
(25) Ryu, M. H.; Kang, I. H.; Nelson, M. D.; Jensen, T. M.; Lyuksyutova, A. I.; Siltberg-Liberles, J.; Raizen, D. M.; Gomelsky, M. Engineering adenylate cyclases regulated by near-infrared window light. *Proc. Natl. Acad. Sci. U. S. A.* **2014**, *111*, 10167−10172.
(26) Camacho-Soto, K.; Castillo-Montoya, J.; Tye, B.; Ogunleye, L. O.; Ghosh, I. Small molecule gated split-tyrosine phosphatases and orthogonal split-tyrosine kinases. *J. Am. Chem. Soc.* **2014**, *136*, 17078−17086.
(27) Dagliyan, O.; Krokhotin, A.; Ozkan-Dagliyan, I.; Deiters, A.; Der, C. J.; Hahn, K. M.; Dokholyan, N. V. Computational design of chemogenetic and optogenetic split proteins. *Nat. Commun.* **2018**, *9*, No. 4042.
(28) Bogomolovas, J.; Simon, B.; Sattler, M.; Stier, G. Screening of fusion partners for high yield expression and purification of bioactive viscotoxins. *Protein Expression Purif.* **2009**, *64*, 16−23.
(29) Nallamsetty, S.; Waugh, D. S. Solubility-enhancing proteins MBP and NusA play a passive role in the folding of their fusion partners. *Protein Expression Purif.* **2006**, *45*, 175−182.
(30) Ren, L.; Chen, X.; Luechapanichkul, R.; Selner, N. G.; Meyer, T. M.; Wavreille, A.-S.; Chan, R.; Iorio, C.; Zhou, X.; Neel, B. G.; Pei, D. Substrate Specificity of Protein Tyrosine Phosphatases 1B, RPTPα, SHP-1, and SHP-2. *Biochemistry* **2011**, *50*, 2339−2356.
(31) Gavin, J. R.; Roth, J.; Neville, D. M.; De Meyts, P.; Buell, D. N. Insulin-Dependent Regulation of Insulin Receptor Concentrations: A Direct Demonstration in Cell Culture. *Proc. Natl. Acad. Sci. U. S. A.* **1974**, *71*, 84−88.
(32) Strickland, D.; Yao, X.; Gawlak, G.; Rosen, M. K.; Gardner, K. H.; Sosnick, T. R. Rationally improving LOV domain-based photoswitches. *Nat. Methods* **2010**, *7*, 623−6.
(33) van Rosmalen, M.; Krom, M.; Merkx, M. Tuning the Flexibility of Glycine-Serine Linkers To Allow Rational Design of Multidomain Proteins. *Biochemistry* **2017**, *56*, 6565−6574.
(34) Barr, A. J.; Ugochukwu, E.; Lee, W. H.; King, O. N. F.; Filippakopoulos, P.; Alfano, I.; Savitsky, P.; Burgess-Brown, N. A.; Müller, S.; Knapp, S. Large-Scale Structural Analysis of the Classical Human Protein Tyrosine Phosphatome. *Cell* **2009**, *136*, 352−363.
(35) Hjortness, M. K.; Riccardi, L.; Hongdusit, A.; Ruppe, A.; Zhao, M.; Kim, E. Y.; Zwart, P. H.; Sankaran, B.; Arthanari, H.; Sousa, M. C.; De Vivo, M.; Fox, J. M. Abietane-Type Diterpenoids Inhibit Protein Tyrosine Phosphatases by Stabilizing an Inactive Enzyme Conformation. *Biochemistry* **2018**, *57*, 5886−5896.
(36) Galic, S.; Klingler-Hoffmann, M.; Fodero-Tavoletti, M. T.; Puryer, M. A.; Meng, T.-C.; Tonks, N. K.; Tiganis, T. Regulation of insulin receptor signaling by the protein tyrosine phosphatase TCPTP. *Mol. Cell. Biol.* **2003**, *23*, 2096−2108.
(37) Dyson, M. R.; Shadbolt, S. P.; Vincent, K. J.; Perera, R. L.; McCafferty, J. Production of soluble mammalian proteins in Escherichia coli: identification of protein features that correlate with successful expression. *BMC Biotechnol.* **2004**, *4*, 32.
(38) Hallett, R. A.; Zimmerman, S. P.; Yumerefendi, H.; Bear, J. E.; Kuhlman, B. Correlating in Vitro and in Vivo Activities of Light-Inducible Dimers: A Cellular Optogenetics Guide. *ACS Synth. Biol.* **2016**, *5*, 53−64.
(39) Dodd, G. T.; Decherf, S.; Loh, K.; Simonds, S. E.; Wiede, F.; Balland, E.; Merry, T. L.; Münzberg, H.; Zhang, Z.-Y.; Kahn, B. B.; Neel, B. G.; Bence, K. K.; Andrews, Z. B.; Cowley, M. A.; Tiganis, T. Leptin and Insulin Act on POMC Neurons to Promote the Browning of White Fat. *Cell* **2015**, *160*, 88−104.
(40) Hjortness, M. K.; Riccardi, L.; Hongdusit, A.; Zwart, P. H.; Sankaran, B.; De Vivo, M.; Fox, J. M. Evolutionarily Conserved Allosteric Communication in Protein Tyrosine Phosphatases. *Biochemistry* **2018**, *57*, 6443−6451.

https://doi.org/10.1021/acssynbio.1c00398
ACS Synth. Biol. 2022, 11, 61−68